GEOPHYSICS, VOL. 75, NO. 6 (NOVEMBER-DECEMBER 2010); P. R129–R136, 11 FIGS.
10.1190/1.3507237

Applications of multiscale waveform inversion to marine data using a flooding technique and dynamic early-arrival windows

Chaiwoot Boonyasiriwat[1], Gerard T. Schuster[1], Paul Valasek[2], and Weiping Cao[3]

ABSTRACT

A recently developed time-domain multiscale waveform tomography (MWT) method is applied to synthetic and field marine data. Although the MWT method was already applied to synthetic data, the synthetic data application leads to a development of a hybrid method between waveform tomography and the salt flooding technique commonly use in subsalt imaging. This hybrid method can overcome a convergence problem encountered by inversion with a traveltime velocity tomogram and successfully provides an accurate and highly resolved velocity tomogram for the 2D SEG/EAGE salt model. In the application of MWT to the field data, the inversion process is carried out using a multiscale method with a dynamic early-arrival muting window to mitigate the local minima problem of waveform tomography and elastic effects. With the modified MWT method, reasonably accurate results as verified by comparison of migration images and common image gathers were obtained. The hybrid method with the salt flooding technique is not used in this field data example because there is no salt in the subsurface according to our interpretation. However, we believe it is applicable to field data applications.

INTRODUCTION

Accurate velocity models of subsurface structures are required to obtain reliable migration images of the subsurface for both time- and depth-domain seismic imaging methods. For example, in areas with rugged surface topography and complex near-surface structures, conventional time-domain methods are likely to fail due to the statics problem. With an accurate velocity model, a tomostatics method can improve the quality of the stacked section. The role of velocity models is even more crucial in the depth domain where conventional prestack depth migration methods normally yield unreliable migration images unless the velocity model is accurate.

The standard tools for more accurate velocity estimation include traveltime tomography (Zhu and McMechan, 1989; Luo and Schuster, 1991; Pratt and Goulty, 1991; Schuster and Quintus-Bosz, 1993; Nemeth et al., 1997; Min and Shin, 2006) and migration velocity analysis (Stork, 1992; Tieman, 1995; Jiao et al., 2002; Sava et al., 2005; Sava and Vlad, 2008). Traveltime tomography is computationally efficient, but forward modeling with ray tracing, which involves a high-frequency approximation, conflicts with the band-limited nature of seismic sources. The widely used MVA methods usually require intensive quality control and typically provide just a smooth velocity model. In contrast, waveform tomography directly inverts the seismic waveform data and can provide accurate and highly resolved velocity models (Bunks et al., 1995; Zhou et al., 1995, 1997; Sheng et al., 2006; Sirgue et al., 2008; Boonyasiriwat et al., 2009a).

Waveform tomography is a highly nonlinear inverse problem and tends to converge to a local minimum if the starting model is not in the vicinity of the global minimum (Gauthier et al., 1986). Therefore, a good initial velocity model is required by waveform tomography to partially overcome the local minima problem. To further mitigate the nonlinearity of waveform tomography, Bunks et al. (1995) introduced a multiscale method that sequentially inverts data band-passed from lower to higher frequencies. Once the smooth or low-wavenumber velocity structures are reconstructed, the higher-wavenumber structures are reconstructed using higher-frequency data. Boonyasiriwat et al. (2009a) improved the multiscale method of Bunks et al. (1995) by using more efficient low-pass filters and a strategy for choosing optimal frequency bands based on the original work of Sirgue and Pratt (2004). Using the modified time-domain multiscale method, Boonyasiriwat et al. (2009b) successfully invert-

Manuscript received by the Editor 7 July 2009; revised manuscript received 17 April 2010; published online 13 December 2010.
[1]Formerly at University of Utah, Department of Geology and Geophysics, Salt Lake City, Utah, U.S.A., presently at King Abdullah University of Science and Technology, Division of Physical Science and Technology, Thuwal, Saudi Arabia. E-mail: chaiwoot@yahoo.com; gerard.schuster@kaust.edu.sa.
[2]Formerly at ConocoPhillips, Subsurface Technology, Houston, Texas, U.S.A., presently at ConocoPhillips, Aberdeen, U. K. E-mail: Paul.A.Valasek@conocophillips.com.
[3]Formerly at University of Utah, Department of Geology and Geophysics, Salt Lake City, Utah, U.S.A., presently at Chevron, Houston, Texas, U.S.A. E-mail: caoweiping 2004@yahoo.com.cn.
© 2010 Society of Exploration Geophysicists. All rights reserved.

Downloaded 04 Mar 2012 to 109.171.137.210. Redistribution subject to SEG license or copyright; see Terms of Use at http://segdl.org/

ed a synthetic data set generated from a Canadian-Foothills velocity model that had a rugged surface topography and complex subsurface structures.

In this work, we present two specialized modifications of the multiscale waveform tomography (MWT) of Boonyasiriwat et al. (2009a), one to synthetic data from the 2D SEG/EAGE salt model, and the other to field data from the Gulf of Mexico. In the synthetic application, the MWT method has a convergence problem and fails to provide an accurate result. Then, we use a flooding method ("flooding" is a technique common in subsalt migration) to overcome the convergence problem, which could be due to a large velocity contrast in the medium. The results of this experiment distinguish this work from our previously published work and possibly others; e.g., Shin and Ha (2008) also applied a Fourier-Laplace waveform inversion method to the 2D SEG/EAGE salt model, but their inversion result (Figure 19b) did not contain the salt body as accurate as our result. In the field data application from the Gulf of Mexico, the S-waves and converted waves in the data are considered as coherent noise due to the acoustic waveform inversion method used in this work. To avoid a convergence or artifact problem, we reduce the elastic influences in the data by using MWT with a dynamic early-arrival muting window. This strategy was also used in a blind test of a frequency-domain method (Brenders and Pratt, 2007). In addition, a static early-arrival muting window is previously used in time-domain waveform inversion by Sheng et al. (2006) without a multiscale strategy, whereas Shipp and Singh (2002) used a multiscale, multistaged method. In our work, we also use a multiscale method with a dynamic early-arrival muting window. Numerical results in this experiment suggest that our method can also be successfully applied to the field data to obtain an accurate velocity model for depth-domain seismic imaging.

MULTISCALE EARLY-ARRIVAL WAVEFORM TOMOGRAPHY

In this section, we present a time-domain implementation of multiscale waveform tomography (MWT). More details on the theory of time-domain waveform tomography are described in Tarantola (1984) and Boonyasiriwat et al. (2009a). In the frequency domain, the data are decomposed into separate frequency components, and it is straightforward to apply the multiscale method. In contrast, time-domain inversion simultaneously uses multiple frequency components of the data in a frequency band. Thus, the data must be band-pass filtered into multiple frequency bands with various peak frequencies, and the inversion process can proceed using low-frequency data and then high-frequency data.

A Wiener filter is used for low-pass filtering the data; Boonyasiriwat et al. (2009a) show that Wiener filtering is more accurate than the filtering method proposed by Bunks et al. (1995). A low-pass Wiener filter (Boonyasiriwat et al., 2009a) can be computed by

$$f_{\text{Wiener}}(\omega) = \frac{W_{\text{target}}(\omega) W^{\dagger}_{\text{original}}(\omega)}{|W_{\text{original}}(\omega)|^2 + \epsilon^2}, \tag{1}$$

where f_{Wiener} is the Wiener filter, W_{original} is the original wavelet, W_{target} is the low-frequency target wavelet, ω is an angular frequency, ϵ is a damping factor to prevent numerical instability, and $\dagger$ denotes the complex conjugate. The Wiener filter is applied to the source wavelet and data in the frequency domain.

Once the source and data are filtered to a low-frequency band, the spacing of the finite-difference grid points can be determined by the maximum frequency of the band. The numerical dispersion condition for the finite-difference scheme used in this work requires at least five grid points per minimum wavelength (Levander, 1988). A square grid ($dx = dz$) is used in the finite-difference scheme so that the grid spacing dx is determined by

$$dx \le \frac{\lambda_{\min}}{5} \le \frac{c_{\min}}{5 f_{\max}}, \tag{2}$$

where $\lambda_{\min}$ is the minimum wavelength, $c_{\min}$ is the minimum velocity, and $f_{\max}$ is the maximum frequency of the band. At low frequencies, coarser grids can be used than those at high frequencies. Therefore, low-frequency inversions will be fast and efficient compared to high-frequency inversions and can afford to take a large number of iterations in order to obtain an accurate estimate of low-wavenumber components in the velocity model.

The multiscale approach has the ability to mitigate the local minima problem commonly encountered in waveform tomography (Bunks et al., 1995; Boonyasiriwat et al., 2009a). The velocity model with accurate low-wavenumber components is a good initial model for higher-frequency inversions, whereas higher-frequency data progressively recover the higher-wavenumber parts of the model.

In practice, our acoustic modeling does not account for elastic effects in the data, attenuation, unknown density, unknown source wavelet, and source radiation patterns, which can lead to a poor convergence. We try to partly overcome these problems by using a multiscale method with a dynamic early-arrival muting window, which partly corrects for attenuation and wavelet distortion effects. The inversion initially inverts data low-pass filtered and windowed about a short time window. After some iterations, higher-frequency data are used in the inversion with the same muting window. Then, the inversion proceeds with longer time windows.

NUMERICAL RESULTS

To demonstrate its effectiveness, we apply MWT to synthetic data from the 2D SEG/EAGE salt model and to marine data from the Gulf of Mexico.

2D SEG/EAGE Salt Model

The 2D SEG/EAGE salt model (Figure 1a) has dimensions of 16 $\times$ 3.7 km with a source spacing of 40 m and a receiver spacing of 20 m. Sources and receivers are located along the free surface. We use two initial models: the first one is from traveltime tomography (Figure 1b), and the second one is the $v(z)$ model (Figure 1c) obtained from a smooth 1D sediment velocity profile of the true model. The traveltime inversion method used in this work is the refraction traveltime inversion method with dynamic smoothing filters of (Nemeth et al., 1997). The original data are generated using a 20-Hz Ricker wavelet with a maximum offset of 16 km. A common shot gather from a source at the center of the free surface is shown in Figure 2a. To use the multiscale method, the original data are low-pass filtered to two frequency bands with peak frequencies of 2.5 and

Downloaded 04 Mar 2012 to 109.171.137.210. Redistribution subject to SEG license or copyright; see Terms of Use at http://segdl.org/

5 Hz; the filtered data are shown in Figure 2b and c, and the MWT results are shown in Figure 3. In the inversion of the 2.5-Hz data, the number of model parameters to be estimated is 403×94, and the grid spacing is 40 m. The number of model parameters to be estimated in the inversion of the 5-Hz data is 806×187, and the grid spacing is 20 m. Using the traveltime tomogram (Figure 1b), MWT converges to a local minimum and provides an inaccurate velocity tomogram (Figure 3b). We believe this is due to inaccurate velocity values above the tip of the salt body at $x = 9$ km. Waveform inversion could not recover both the low velocity zone above the salt and the velocity of the salt body. Consequently, it produces a high-velocity artifact at the location of the salt tip, which clearly affects the recovery of the salt body in the neighboring regions and causes the inversion to converge to a local minimum far from the global minimum (true velocity model).

In contrast to the traveltime tomogram, the $v(z)$ model has roughly accurate sediment velocities, especially at the location above the tip of the salt body, but has no information about the salt body. If only the $v(z)$ model is used, we can accurately recover the top boundary of the salt body and its rough estimate. An accurate and highly resolved velocity tomogram (Figure 3c) is obtained when the $v(z)$ model is used with a flooding technique.

Now we explain how the flooding technique yielded the above tomogram. Using the $v(z)$ model, the inversion was iterated for 100 iterations and yielded the tomogram shown in Figure 4a. Note that there is no artifact at the tip of the salt as in the case where the traveltime tomogram is used. After the top of the salt boundary is picked, the salt velocity of 4500 m/s is used to flood the region below the salt's top boundary, and the resulting velocity (Figure 4b) is used to migrate the data. At this step, we assume that the salt velocity is previously estimated by some method, e.g., the method proposed by Young et al. (1999). Although an accurate salt velocity is used here in this test, the use of inaccurate salt velocity would only affect the location of the bottom of the salt body. In this paper, the bottom of the salt body is crudely picked from the migration image (not shown here) so its location is incorrect. The location of the bottom of the salt is gradually corrected through inversion. To verify this conjecture, we use a wrong salt velocity with 10% error during the flooding process, and the inversion still provides a velocity tomography with an accurate salt body and subsalt structure. The velocity model in Figure 4b obtained after the salt flood is flooded with a sediment velocity of 3000 m/s below the salt bottom to obtain the velocity model shown in Figure 4c. This sediment velocity is arbitrarily picked from the initial model at the same depth. Then the velocity model obtained

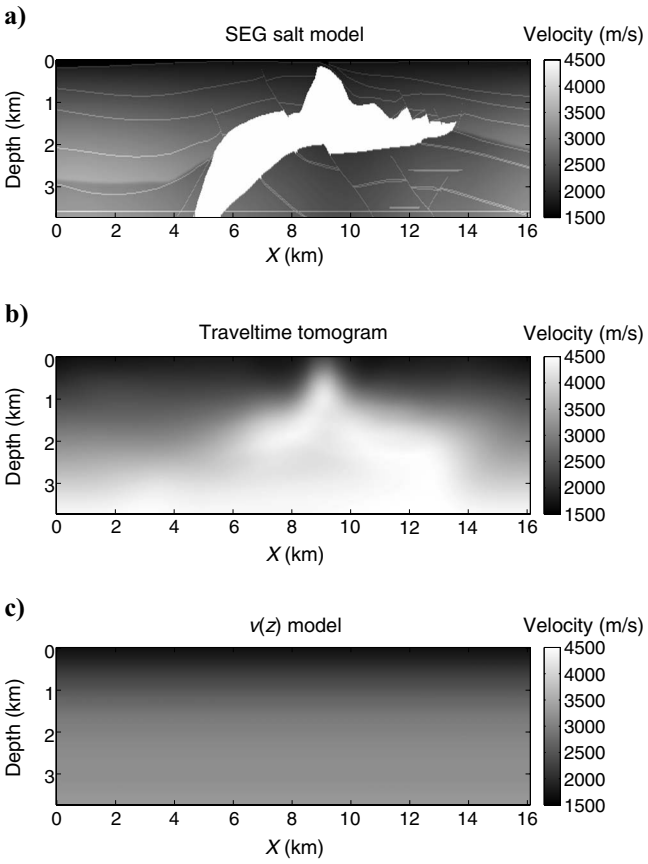

Figure 1. The 2D SEG/EAGE salt model and initial models. (a) The salt model. (b) Traveltime velocity model. (c) $v(z)$ velocity model.

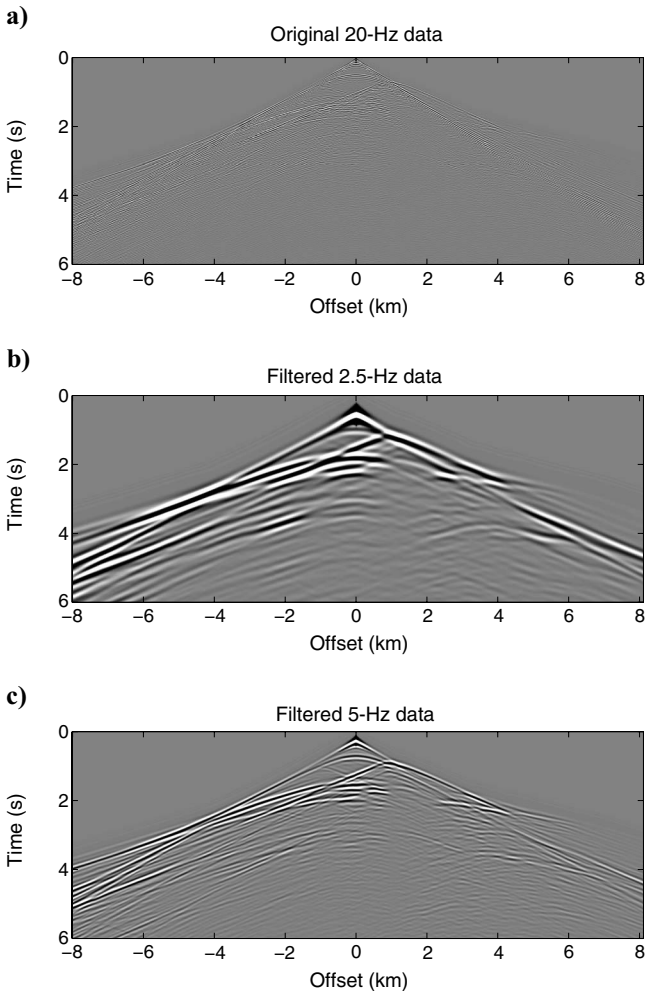

Figure 2. Synthetic data from the 2D SEG/EAGE salt model. (a) Original 20-Hz data. (b) Filtered 2.5-Hz data. (c) Filtered 5-Hz data.

Downloaded 04 Mar 2012 to 109.171.137.210. Redistribution subject to SEG license or copyright; see Terms of Use at http://segdl.org/

after the flooding process is used as an initial model for another inversion, which was iterated for 30 iterations. The data residuals from both inversion processes are shown in Figure 5. The waveform tomogram from the 2.5-Hz data is then is used as an initial model for inverting 5-Hz data, and the final velocity model is obtained as shown in Figure 3c. The residual plot using 5-Hz data is shown in Figure 6.

Gulf of Mexico

In this section, we apply multiscale acoustic waveform inversion to a streamer data set from the Gulf of Mexico acquired using 515 shots with a shot interval of 37.5 m, a time-sampling interval of 2 ms, a trace length of 10 s, and 480 active hydrophones per shot. The hydrophone interval is 12.5 m, with a near offset of 198 m and a far offset of about 6 km.

Prior to applying waveform inversion, the data are transformed from 3D to 2D format by applying the filter $\sqrt{i/\omega}$ in the frequency domain to correct for 3D geometrical spreading (Zhou et al., 1995). Noise in the data before first arrivals are muted, the attenuation factor Q is estimated by the spectral ratio method (Maresh et al., 2006), and the attenuation effect is compensated by applying an inverse-Q filter (Wang, 2006) to the data. In contrast to the data processing of Hicks and Pratt (2001), we did not apply multiple attenuation to the data. The source wavelet is estimated by stacking along the water-bottom reflection. Then, the data are low-pass filtered to two frequency bands with passbands of 0–15 and 0–25 Hz using the method proposed by Boonyasiriwat et al. (2009a). Figure 7a and b shows the original and filtered shot gathers, respectively. Only the P-wave velocity is inverted for, and the density is estimated using an empirical formula (Gardner et al., 1974).

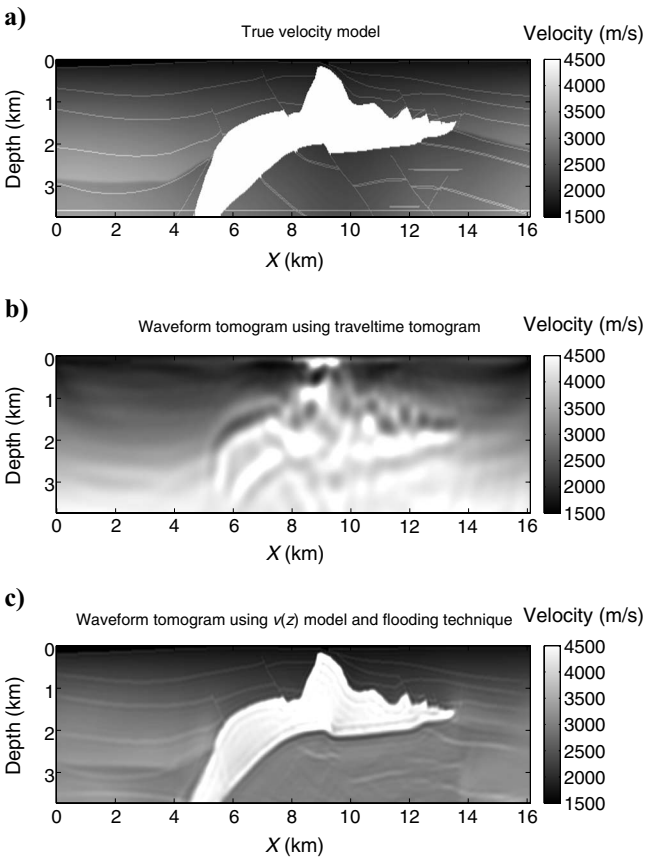

Figure 3. Waveform inversion results. (a) True model. (b) Waveform tomogram using the traveltime tomogram and 2.5-Hz data. (c) Waveform tomogram using the $v(z)$ model, the flooding technique, and 2.5-Hz and 5-Hz data.

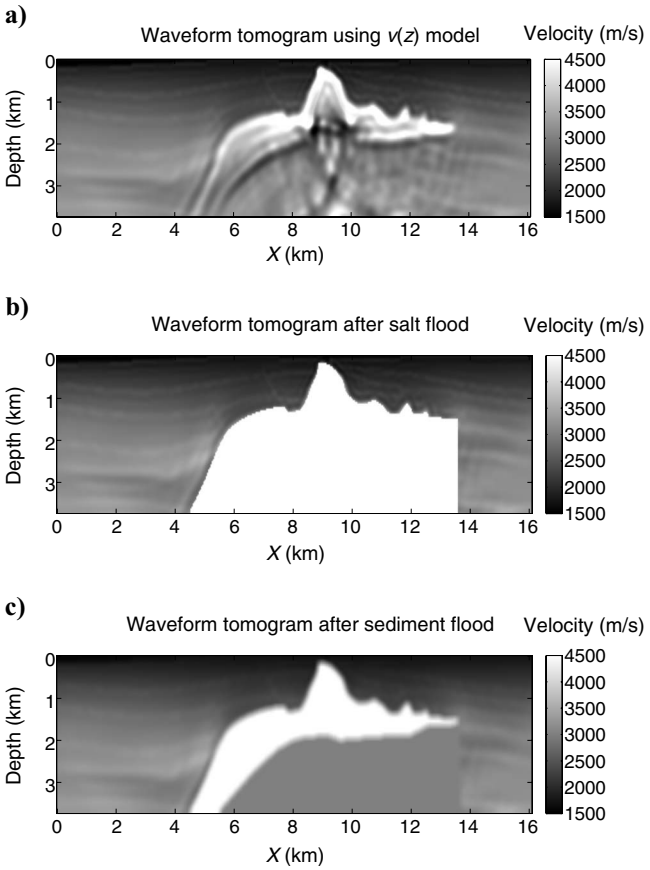

Figure 4. Flooding process. (a) Waveform tomogram using only the $v(z)$ model. (b) Velocity model obtained after a salt flood of the waveform tomogram in (a). (c) Velocity model obtained after salt and sediment floods of the waveform tomogram in (a).

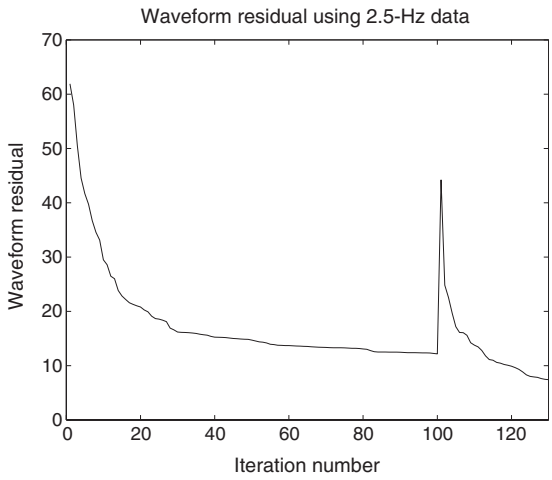

Figure 5. Waveform residual plot using 2.5-Hz synthetic data.

Downloaded 04 Mar 2012 to 109.171.137.210. Redistribution subject to SEG license or copyright; see Terms of Use at http://segdl.org/

In this real data example, there is no salt in the subsurface structures so the hybrid method presented in the synthetic data example is not used in this case. However, there are still some challenges in inverting real data including elastic and attenuation effects, unknown source signature, and random and coherent noise. These issues normally cause waveform inversion to be much more challenging in real data cases than in synthetic ones, and extra processing steps or strategies are normally required for successful inversion.

Traveltime tomography is utilized to provide an initial velocity model for waveform tomography (Figure 8a). The inversion process is composed of three parts, and in each part a muting window with a different length is used for inversion of both the low- and high-pass data. In the first part, a muting window of length 1 s is applied to the filtered data, and the inversion sequentially proceeds using data with passbands of 0–15 and 0–25 Hz. The reconstructed velocity from the first part is used as an initial model in the second part where a 2-s window is used, and, in the last part, a 3-s window is applied. Figure 8b shows the reconstructed velocity tomogram from waveform tomography, which has a higher resolution than the initial model (Figure 8a). The predicted shot gathers obtained by using traveltime tomogram and waveform tomogram are shown in Figure 7c and d, respectively.

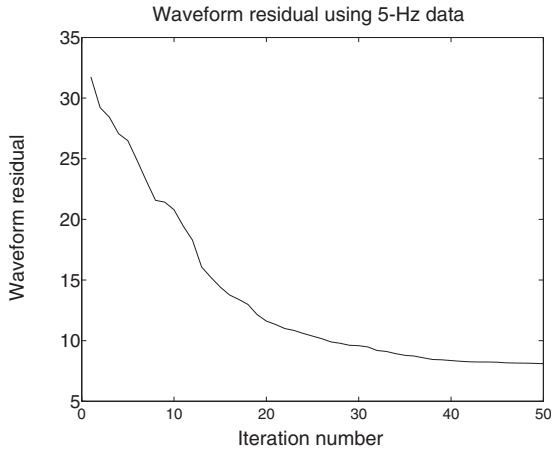

Figure 6. Waveform residual plot using 5-Hz synthetic data.

To verify that the reconstructed velocity tomogram is more accurate than the initial model, we compare the migration images and common image gathers (CIG) obtained by using the initial model and the final model. The original data were migrated using Kirchhoff migration and the migration images using the traveltime and waveform tomograms are shown in Figure 9a and b, respectively. The zoomed views of the migration images are shown in Figure 10 for more detailed comparisons. Using the waveform tomogram as the migration velocity, the resulting migration image appears to be better focused than that obtained by using the traveltime tomogram as the migration velocity. Comparing the CIGs in Figure 11, the waveform tomogram is more accurate than the traveltime tomogram because the corresponding CIGs are flatter. Horizontal reflectors in a common image gather are an indication that the migration velocity model is accurate (Yilmaz, 2001). Although most CIGs are flatter when the waveform tomogram is used, some CIGs on the right part are less flat. This means that the model is less accurate in this region. The reasons for this could be due to the edge effect, more complex subsurface structures or sea floor in this area. Further study may also be needed to accurately explain this result, and further development of our inversion method is still needed to improve the inversion results.

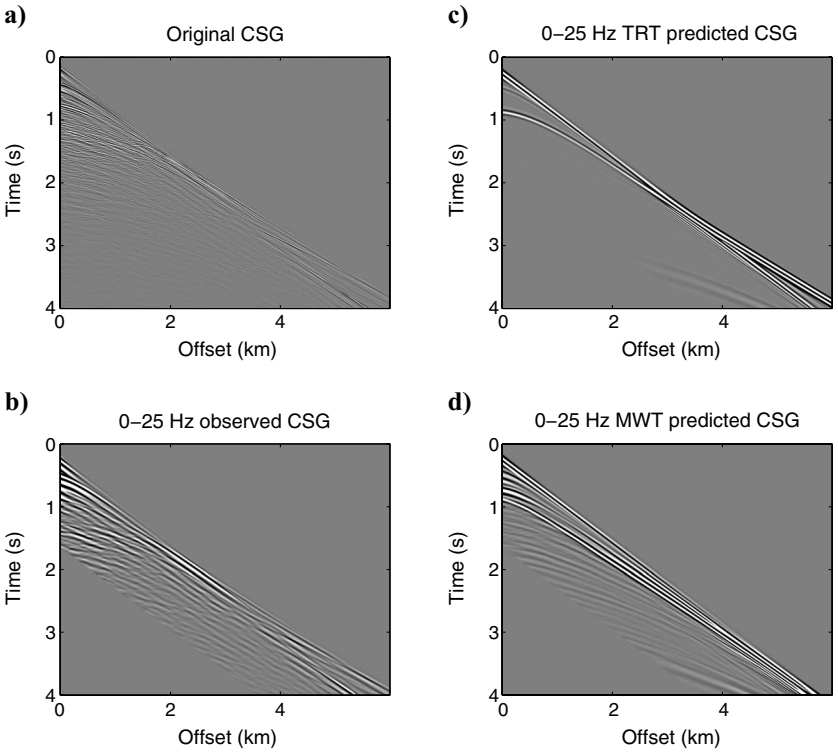

Figure 7. Marine data. (a) An original CSG from a source at $x = 0$ km. The white line is the picked first-arrival traveltimes. (b) A filtered shot gather with a passband of 0–25 Hz. (c) A predicted shot gather obtained by using the traveltime tomogram. (d) A predicted shot gather obtained by using the waveform tomogram.

Downloaded 04 Mar 2012 to 109.171.137.210. Redistribution subject to SEG license or copyright; see Terms of Use at http://segdl.org/

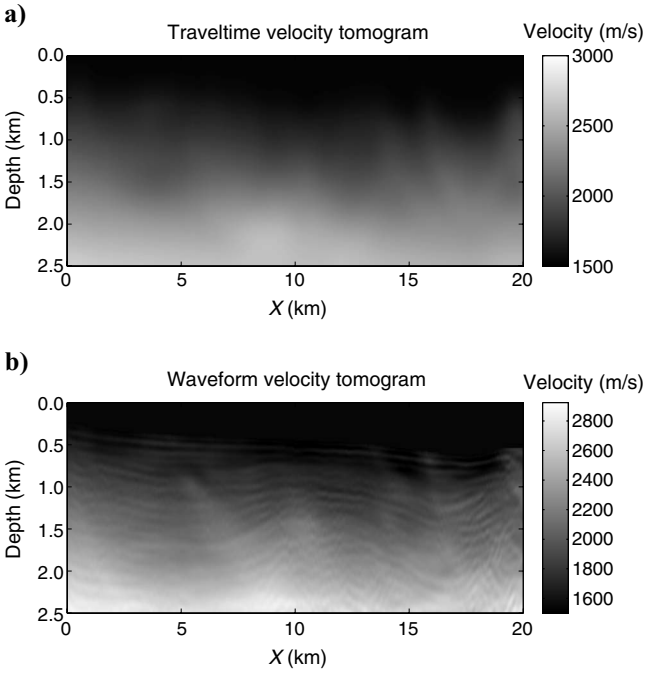

Figure 8. Inversion results from the marine data. (a) The initial velocity model obtained from traveltime tomography. (b) The velocity tomogram obtained from waveform tomography.

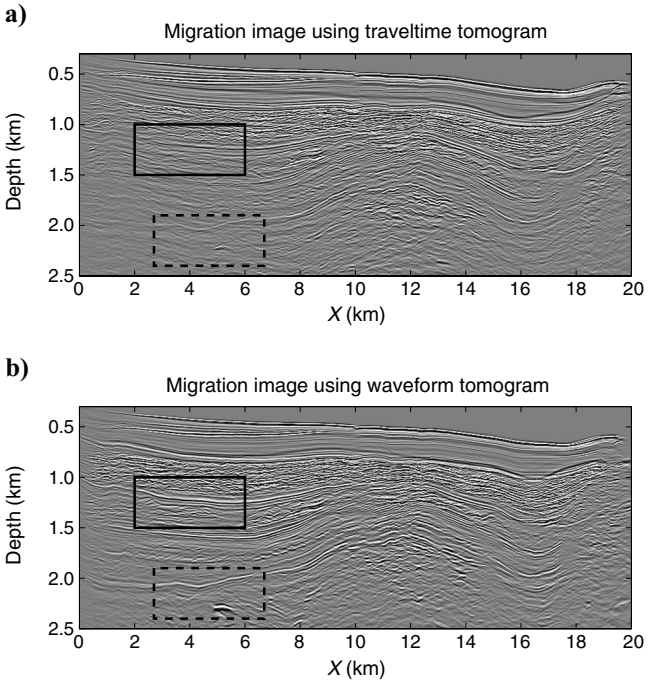

Figure 9. Migration images from the marine data. (a) The Kirchhoff migration image obtained using the original data and the traveltime tomogram. (b) The Kirchhoff migration image obtained using the waveform tomogram.

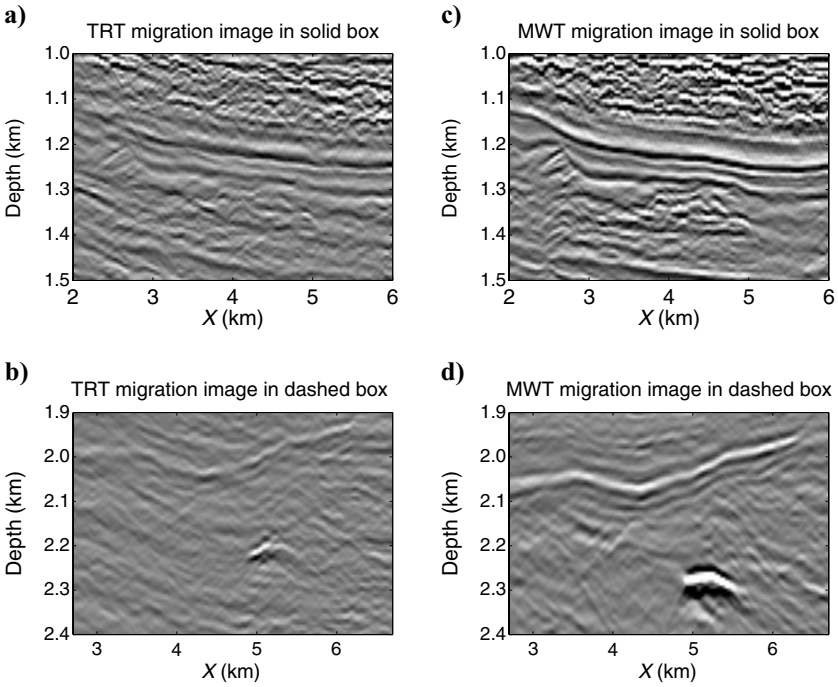

Figure 10. Zoomed views of migration images from the marine data. Using the traveltime tomogram, the Kirchhoff migration images in (a) the solid box and (b) the dashed box are obtained. Using the waveform tomogram, the Kirchhoff migration image in (c) the solid box and (d) the dashed box are obtained.

Downloaded 04 Mar 2012 to 109.171.137.210. Redistribution subject to SEG license or copyright; see Terms of Use at http://segdl.org/

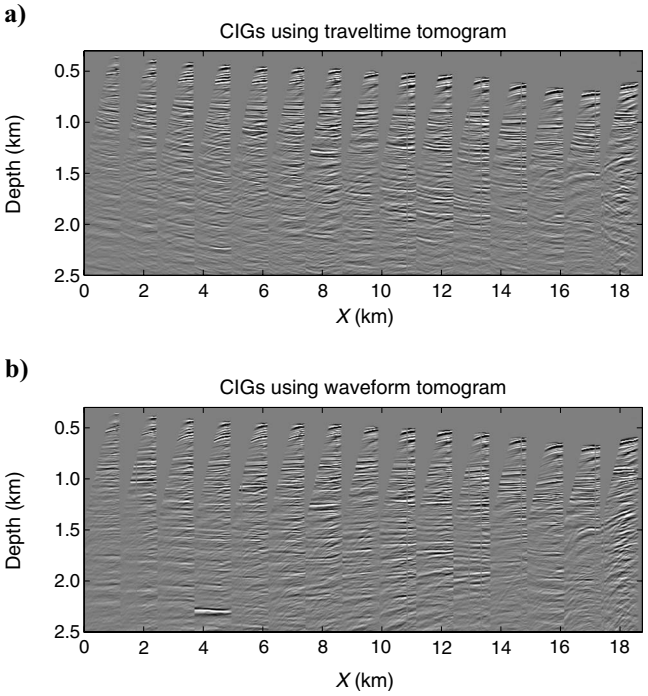

Figure 11. Common image gathers (CIGs) obtained from the marine data migrated with the (a) traveltime tomogram and (b) waveform tomogram as the velocity model.

CONCLUSIONS

Acoustic waveform tomography is used to invert both 2D synthetic and field data for the velocity models. In the case of 2D synthetic data from the SEG/EAGE salt model, the traveltime velocity model is not a good starting model for waveform inversion as it causes artifacts at the tip of the salt body. We believe this is due to the inaccuracy of the traveltime tomogram above the tip of the salt body and the resolution limit of low-frequency inversion using 2.5-Hz data. Consequently, waveform inversion converged to a local minimum that was inaccurate compared to the true model. To overcome this problem, we discovered that the flooding technique, commonly used in subsalt imaging, can be used to improve the convergence of waveform inversion. Surprisingly, combining the $v(z)$ velocity model, which is only a 1D velocity profile with a good estimate of sediment velocity profiles, with the flooding technique can provide an accurate velocity model by multiscale waveform tomography.

In the marine data case, multiscale waveform tomogram with a dynamic early-arrival muting window successfully inverted the marine data set to obtain a velocity tomogram that is more accurate than the initial model from traveltime tomography. Because in this case, the true velocity structure is not known, the accuracy of the waveform tomogram is assessed by comparing the migration images and common image gathers. The results showed that acoustic waveform tomography can be used to invert these elastic field data. This success is attributed to the fact that marine data are simpler than land data that are usually corrupted by surface waves, strong random noise, and strong elastic effects.

ACKNOWLEDGMENTS

We are grateful for the support from the members of the University of Utah Tomography and Modeling/Migration Consortium. We also thank Amerada Hess for providing us the marine data set and Partha Routh for help and useful discussions. We thank associate editor Kris Innanen and three anonymous reviewers for their constructive criticisms.

REFERENCES

Boonyasiriwat, C., P. Valasek, P. Routh, W. Cao, G. T. Schuster, and B. Macy, 2009a, An efficient multiscale method for time-domain waveform tomography: Geophysics, **74**, no. 6, WCC59–WCC68, doi: 10.1190/1.3151869.

Boonyasiriwat, C., P. Valasek, P. Routh, and X. Zhu, 2009b, Application of multiscale waveform tomography for high-resolution velocity estimation in complex geologic environments: Canadian Foothills synthetic data example: The Leading Edge, **28**, 454–456, doi: 10.1190/1.3112764.

Brenders, A. J., and R. G. Pratt, 2007, Full waveform tomography for lithospheric imaging: Results from a blind test in a realistic crustal model: Geophysical Journal International, **168**, no. 1, 133–151, doi: 10.1111/j.1365-246X.2006.03156.x.

Bunks, C., F. M. Saleck, S. Zaleski, and G. Chavent, 1995, Multiscale seismic waveform inversion: Geophysics, **60**, 1457–1473, doi: 10.1190/1.1443880.

Gardner, G. H. F., L. W. Gardner, and A. R. Gregory, 1974, Formation velocity and density — the diagnostic basics for stratigraphic traps: Geophysics, **39**, 770–780, doi: 10.1190/1.1440465.

Gauthier, O., J. Virieux, and A. Tarantola, 1986, Two-dimensional nonlinear inversion of seismic waveforms: Numerical results: Geophysics, **51**, 1387–1403, doi: 10.1190/1.1442188.

Hicks, G., and R. G. Pratt, 2001, Reflection waveform inversion using local descent methods: Estimating attenuation and velocity over a gas-sand deposit: Geophysics, **66**, 598–612, doi: 10.1190/1.1444951.

Jiao, J., P. L. Stoffa, M. K. Sen, and R. K. Seifoullaev, 2002, Residual migration-velocity analysis in the plane-wave domain: Geophysics, **67**, 1258–1269, doi: 10.1190/1.1500388.

Levander, A., 1988, Fourth-order finite-difference P-SV seismograms: Geophysics, **53**, 1425–1437, doi: 10.1190/1.1442422.

Luo, Y., and G. T. Schuster, 1991, Wave equation traveltime inversion: Geophysics, **56**, 645–653, doi: 10.1190/1.1443081.

Maresh, J., R. S. White, R. W. Hobbs, and J. R. Smallwood, 2006, Seismic attenuation of Atlantic margin basalts: Observations and modeling: Geophysics, **71**, no. 6, B211–B221, doi: 10.1190/1.2335875.

Min, D., and C. Shin, 2006, Refraction tomography using a waveform-inversion back-propagation technique: Geophysics, **71**, no. 3, R21–R30, doi: 10.1190/1.2194522.

Nemeth, T., E. Normark, and F. Qin, 1997, Dynamic smoothing in cross-well traveltime tomography: Geophysics, **62**, 168–176, doi: 10.1190/1.1444115.

Pratt, R. G., and N. R. Goulty, 1991, Combining wave-equation imaging with traveltime tomography to form high-resolution images from crosshole data: Geophysics, **56**, 208–224, doi: 10.1190/1.1443033.

Sava, P., B. Biondi, and J. Etgen, 2005, Wave-equation migration velocity analysis by focusing diffractions and reflections: Geophysics, **70**, no. 3, U19–U27, doi: 10.1190/1.1925749.

Sava, P., and I. Vlad, 2008, Numeric implementation of wave-equation migration velocity analysis operators: Geophysics, **73**, no. 5, VE145–VE159, doi: 10.1190/1.2953337.

Schuster, G. T., and A. Quintus-Bosz, 1993, Wavepath eikonal traveltime inversion: Theory: Geophysics, **58**, 1314–1323, doi: 10.1190/1.1443514.

Sheng, J., A. Leeds, M. Buddensiek, and G. T. Schuster, 2006, Early arrival waveform tomography on near-surface refraction data: Geophysics, **71**, no. 4, U47–U57, doi: 10.1190/1.2210969.

Shin, C., and W. Ha, 2008, A comparison between the behavior of objective functions for waveform inversion in the frequency and Laplace domains: Geophysics, **73**, no. 5, VE119–VE133, doi: 10.1190/1.2953978.

Shipp, R. M., and S. C. Singh, 2002, Two-dimensional full wavefield inversion of wide-aperture marine seismic streamer data: Geophysical Journal International, **151**, no. 2, 325–344, doi: 10.1046/j.1365-246X.2002.01645.x.

Sirgue, L., J. T. Etgen, and U. Albertin, 2008, 3D frequency-domain waveform inversion using time-domain finite-difference methods Presented at the 70th Annual International Meeting, EAGE.

Sirgue, L., and R. G. Pratt, 2004, Efficient waveform inversion and imaging: A strategy for selecting temporal frequencies: Geophysics, **69**, 231–248, doi: 10.1190/1.1649391.

Stork, C., 1992, Reflection tomography in the postmigrated domain: Geophysics, **57**, 680–692, doi: 10.1190/1.1443282.

Tarantola, A., 1984, Inversion of seismic reflection data in the acoustic approximation: Geophysics, **49**, 1259–1266, doi: 10.1190/1.1441754.

Tieman, H. J., 1995, Migration velocity analysis: Accounting for the effects

Downloaded 04 Mar 2012 to 109.171.137.210. Redistribution subject to SEG license or copyright; see Terms of Use at http://segdl.org/

of lateral velocity variations: Geophysics, **60**, 164–175, doi: 10.1190/1.1443743.
Wang, Y., 2006, Inverse Q-filter for seismic resolution enhancement: Geophysics, **71**, no. 3, V51–V60, doi: 10.1190/1.2192912.
Yilmaz, O., 2001, Seismic data analysis — Processing, inversion, and interpretation of seismic data: SEG.
Young, K. T. J., C. D. Notfors, X. G. Meng, and P. Montecchi, 1999, Subsalt imaging in Walker Ridge, Gulf of Mexico: 69th Annual International Meeting, SEG, Expanded Abstracts, 1099–1102, doi: 10.1190/1.1820692.
Zhou, C., W. Cai, Y. Luo, G. T. Schuster, and S. Hassanzadeh, 1995, Acoustic wave-equation traveltime and waveform inversion of crosshole seismic data: Geophysics, **60**, 765–773, doi: 10.1190/1.1443815.
Zhou, C., G. T. Schuster, S. Hassanzadeh, and J. M. Harris, 1997, Elastic wave equation traveltime and waveform inversion of crosswell data: Geophysics, **62**, 853–868, doi: 10.1190/1.1444194.
Zhu, X., and G. A. McMechan, 1989, Estimation of a two-dimensional seismic compressional-wave velocity distribution by iterative tomographic imaging: International Journal of Imaging Systems and Technology, **1**, no. 1, 13–17, doi: 10.1002/ima.1850010103.

Downloaded 04 Mar 2012 to 109.171.137.210. Redistribution subject to SEG license or copyright; see Terms of Use at http://segdl.org/